Exciton states in cylindrical nanowires

2006 J. Phys.: Condens. Matter 18 3951

(http://iopscience.iop.org/0953-8984/18/16/005)

INSTITUTE OF PHYSICS PUBLISHING JOURNAL OF PHYSICS: CONDENSED MATTER

J. Phys.: Condens. Matter **18** (2006) 3951–3966 doi:10.1088/0953-8984/18/16/005

Exciton states in cylindrical nanowires

A F Slachmuylders[1], B Partoens[1], W Magnus[2] and F M Peeters[1]

[1] Departement Fysica, Universiteit Antwerpen, Groenenborgerlaan 171, B-2020 Antwerpen, Belgium
[2] Interuniversity Microelectronics Centre, Kapeldreef 75, B-3001 Leuven, Belgium

Received 27 January 2006
Published 3 April 2006
Online at stacks.iop.org/JPhysCM/18/3951

Abstract

The exciton ground state and excited state energies are calculated for a model system of an infinitely long cylindrical wire. The effective Coulomb potential between the electron and the hole is studied as function of the wire radius. Within the adiabatic approximation, we obtain 'exact' numerical results for the effective exciton potential and the lowest exciton energy levels which are fitted to simple analytical expressions. Furthermore, we investigated the influence of a magnetic field parallel to the nanowire on the effective potential and the exciton energy.

1. Introduction

Nowadays, semiconductor nanowires with a small diameter can be realized in a fast and cost-effective manner. One of the possible growth techniques, the VLS (vapour–liquid–solid) technique, is a bottom-up technique which appears to be very promising [1]. In this method, a liquid metal cluster acts as a catalyst where reactants dissolve, which leads to the direct growth from the supersaturated alloy droplet. This growth method results in a freestanding nanowire that is not surrounded by any other material, in contrast to the embedded wires.

From a theoretical point of view such semiconductor nanowire structures are very interesting for understanding the role of dimensionality on physical properties. Furthermore, they provide a great potential for several applications, such as transistors [2], diodes [3], memory elements [4], lasers [5, 6], and chemical and biological sensors [7].

These nanowires have a large aspect ratio and can be considered one-dimensional structures. They have a length and a diameter in the micrometre and nanometre range, respectively. Electrons and holes are strongly confined in two directions and there is no confinement in the direction of the axis of the wire. Here we will investigate the exciton binding energy and its lowest excited states. Excitons form the basis of optical properties reflecting the intrinsic nature of low-dimensional systems. As a first step we investigate the potential and energy of the electron–hole pair. Because our aim is to present 'exact' numerical results we will limit ourselves for the moment to the *model* system in which the difference in dielectric constant of the nanowire material and its surrounding is neglected. Only in this

special case are we able to present analytical results. Although for 'stand alone' nanowires the dielectric mismatch in the wire (difference in dielectric constant of the material of the wire and the environment) is important, the study of it will be postponed for further investigations.

In previous work [8], a similar model system was studied, but only the ground exciton state was obtained and no systematic study was presented of the dependence on wire radius, mass of the carriers, magnetic field and of the excited states. Also impurity states—both with and without a magnetic field parallel to the wire axis—were considered in previous papers [9, 10], with the charged impurity fixed to the cylinder axis and with averaging performed only over the electronic motion. The effective potential for the ground state configuration was obtained previously [11][3]—the calculations involved the numerical evaluation of multidimensional integrals—and agrees with our results. One of the aims of the present paper is to give explicit analytical expressions for the effective Coulomb potential that are fitted to these numerical results and are more tractable in later calculations of for example the energy levels of exciton complexes. Furthermore, the binding energy of the exciton is calculated numerically for arbitrary wire thicknesses, while the results of [8] were limited to thin wires. Also the energy of excited exciton states are given and analytical expressions are fitted to the numerical results. Finally, the addition of a magnetic field is another extension which has not been studied in detail before. The effective potential was calculated before for embedded rectangular wires [12] for magnetic fields perpendicular and parallel to the wire axis. The focus of [12] is not on the effective potential, but on the calculation of the exciton energy and a comparison with experiment. In [13] analytical expressions for parabolic confined wires were obtained, which we found could be accurately fitted to our results in the high magnetic field limit. Note that our calculations are very general, since they apply to arbitrary materials provided they can be described within the framework of the effective mass theory.

This paper is organized as follows. In section 2 we consider the single-particle states of the electron and hole. In section 3 we calculate the effective potential of the exciton, using the adiabatic approximation. The numerical results for the effective potential as a function of the interparticle distance are fitted to simple analytical expressions. The exciton energy is calculated numerically and semi-analytically in section 4. The influence of a magnetic field will be investigated in section 5 and our conclusions are presented in section 6.

2. Single-particle states

For completeness we first consider the eigenfunctions and corresponding eigenvalues of a single particle in a circular[4] potential well with radius R. Adopting the effective mass approximation we write the Schrödinger equation as follows:

$$-\frac{\hbar^2}{2m}\vec{\nabla}^2\psi(\vec{r}) + V(\vec{r})\psi(\vec{r}) = E\psi(\vec{r}), \tag{1}$$

where we approximate the confinement potential of the wire by a hard wall potential

$$V(\vec{r}) = \begin{cases} 0 & \text{if } \rho \leqslant R \\ \infty & \text{if } \rho > R, \end{cases} \tag{2}$$

where $\rho = \sqrt{x^2 + y^2}$. For the freestanding wire the potential height is given by the work function which is typically a few eV and therefore very large compared to typical confinement

[3] Note that this paper contains several mistakes in the formulae; the figures, however, are correct, which indicates that the mistakes are typing errors. Nevertheless, one should be careful and not just copy the formulae.

[4] For the sake of simplicity, we took circular symmetry. One can perform similar calculations for square wires and find that the final results, i.e. the effective exciton potential and exciton energy, match the result of a circular wire with radius comparable to half of the side of a square. This was investigated by Zhang and Mascarenhas [14].

energies. The wire is oriented along the z-axis. Since the motion in the z-direction (free particle in that direction) is decoupled from the motion in the (x, y)-plane, and, because of circular symmetry, we have $\psi(\rho, \theta, z) = F(\rho)\mathrm{e}^{-\mathrm{i}l\theta}\mathrm{e}^{\mathrm{i}k_z z}$, where θ is the polar angle. The Schrödinger equation is then reduced to the one-dimensional (1D) equation

$$\rho^2 F(\rho)'' + \rho F(\rho)' + ((k^2 - k_z^2)\rho^2 - l^2)F(\rho) = 0, \tag{3}$$

with $k^2 = 2mE/\hbar^2$. The solutions to this equation are the well known Bessel functions, and taking hard wall boundary conditions into account, one gets for the single-particle wavefunctions

$$\psi_{n,l,k_z}(\rho, \theta, z) = C_{n,l}\mathrm{e}^{-\mathrm{i}l\theta} J_l\left(\frac{\beta_{n,l}}{R}\rho\right)\mathrm{e}^{\mathrm{i}k_z z}, \tag{4}$$

and the corresponding eigenenergies

$$E_{n,l,k_z} = \frac{\hbar^2\beta_{n,l}^2}{2mR^2} + \frac{\hbar^2 k_z^2}{2m}, \tag{5}$$

where $C_{n,l}$ is the normalization constant and $\beta_{n,l}$ is the nth-order zero of the Bessel function $J_l(x)$. The zeros of the Bessel functions are known and can be found in the literature [15]: $\beta_{0,0} = 2.4048$, $\beta_{0,1} = 3.8317$, $\beta_{0,2} = 5.1356$, $\beta_{1,0} = 5.5201$, $\beta_{1,2} = 8.4172$, $\beta_{2,2} = 11.6198, \ldots$. Notice that the first excited state is $|0, 1, k_z\rangle$ and the second one $|0, 2, k_z\rangle$.

3. Effective exciton potential

3.1. Adiabatic approximation

The appropriate Hamiltonian for an exciton in the effective mass approximation is given by

$$H = -\frac{\hbar^2}{2m_\mathrm{e}}\vec{\nabla}_\mathrm{e}^2 + V_\mathrm{e}(x_\mathrm{e}, y_\mathrm{e}) - \frac{\hbar^2}{2m_\mathrm{h}}\vec{\nabla}_\mathrm{h}^2 + V_\mathrm{h}(x_\mathrm{h}, y_\mathrm{h}) + V_\mathrm{C}(\vec{r}_\mathrm{e} - \vec{r}_\mathrm{h}), \tag{6}$$

where m_e (m_h) is the effective mass of the electron (hole), V_e (V_h) is the confinement potential of the electron (hole) and

$$V_\mathrm{C}(\vec{r}_\mathrm{e} - \vec{r}_\mathrm{h}) = -\frac{1}{4\pi\epsilon}\frac{e^2}{\sqrt{(x_\mathrm{e} - x_\mathrm{h})^2 + (y_\mathrm{e} - y_\mathrm{h})^2 + (z_\mathrm{e} - z_\mathrm{h})^2}}, \tag{7}$$

is the Coulomb interaction potential between the electron and the hole. In this case, it is convenient to separate the motion of the two particles into that of the centre of mass of the system and the relative motion, thereby introducing the quantities $Z = (m_\mathrm{e}z_\mathrm{e} + m_\mathrm{h}z_\mathrm{h})/(m_\mathrm{e} + m_\mathrm{h})$, $z = z_\mathrm{e} - z_\mathrm{h}$, $M = m_\mathrm{e} + m_\mathrm{h}$, $\mu = (m_\mathrm{e}m_\mathrm{h})/(m_\mathrm{e} + m_\mathrm{h})$. Now the Hamiltonian can be rewritten as

$$\begin{aligned} H = &-\frac{\hbar^2}{2m_\mathrm{e}}\vec{\nabla}_{x_\mathrm{e}, y_\mathrm{e}}^2 + V_\mathrm{e}(x_\mathrm{e}, y_\mathrm{e}) - \frac{\hbar^2}{2m_\mathrm{h}}\vec{\nabla}_{x_\mathrm{h}, y_\mathrm{h}}^2 + V_\mathrm{h}(x_\mathrm{h}, y_\mathrm{h}) - \frac{\hbar^2}{2M}\frac{\partial^2}{\partial^2 Z} - \frac{\hbar^2}{2\mu}\frac{\partial^2}{\partial^2 z} \\ &- \frac{1}{4\pi\epsilon}\frac{e^2}{\sqrt{(x_\mathrm{e} - x_\mathrm{h})^2 + (y_\mathrm{e} - y_\mathrm{h})^2 + z^2}}. \end{aligned} \tag{8}$$

In the case of strong lateral confinement, the exciton motion along the wire is decoupled form the lateral motion of the particles and we may decouple the wavefunction as follows:

$$\Psi(x_\mathrm{e}, y_\mathrm{e}, x_\mathrm{h}, y_\mathrm{h}, z, Z) = \mathrm{e}^{\mathrm{i}KZ}\phi(z)\psi(x_\mathrm{e}, y_\mathrm{e})\psi(x_\mathrm{h}, y_\mathrm{h}). \tag{9}$$

Because the Coulomb energy in the considered case is much weaker than the single-particle confinement energy, we adopt the adiabatic approximation, thereby taking $\psi(x, y)$ as the above obtained single-particle states. Multiplying equation (8) with $\psi^*(x_\mathrm{e}, y_\mathrm{e})\psi^*(x_\mathrm{h}, y_\mathrm{h})$ from

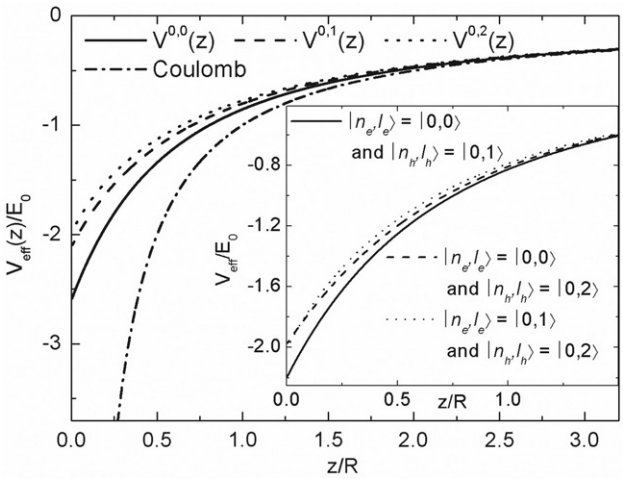

Figure 1. Effective exciton interaction potential as a function of the electron–hole separation z for three different states of the electron and hole (full curve: $n_e = l_e = 0$ and $n_h = l_h = 0$ for the hole; dashed curve: $l_e = l_h = 1$ and $n_e = n_h = 0$; dotted curve: $l_e = l_h = 2$ and $n_e = n_h = 0$). The regular Coulomb potential, $1/z$, is also plotted (dashed–dotted) for comparison. Inset: the effective potential for different sets of quantum numbers for the electron and hole.

the left and with $\psi(x_e, y_e)\psi(x_h, y_h)$ from the right, integrating over the lateral coordinates we reduce the original 6D Schrödinger equation for the exciton problem to a 1D effective Schrödinger equation for the relative exciton coordinate

$$\left(E_e + E_h + \frac{\hbar^2 K^2}{2M} - \frac{\hbar^2}{2\mu}\nabla_z^2 + V_{\text{eff}}(z)\right)\phi(z) = E_{\text{tot}}\phi(z), \tag{10}$$

where E_e (E_h) are the single-electron (hole) energies, and the effective exciton potential, V_{eff}, is given by

$$V_{\text{eff}}^{n,l}(z) = -\frac{e^2}{4\pi\epsilon}\int \mathrm{d}x_e \mathrm{d}x_h \mathrm{d}y_e \mathrm{d}y_h \frac{\left|\psi_{n,l,k_z}(x_e, y_e)\right|^2 \left|\psi_{n,l,k_z}(x_h, y_h)\right|^2}{\sqrt{(x_e - x_h)^2 + (y_e - y_h)^2 + z^2}}. \tag{11}$$

Introducing dimensionless units (i.e. length expressed in units of R) and $\alpha = a_B^*/2R$ with $a_B^* = 4\pi\epsilon\hbar^2/\mu e^2$ the effective Bohr radius, we finally get

$$\left(-\alpha\nabla_z^2 + \tilde{V}_{\text{eff}}(z)\right)\phi(z) = \tilde{E}_C\phi(z), \tag{12}$$

where z is given in units of R, $\tilde{V} = V/E_0$, $\tilde{E}_C = E_C/E_0$, $E_0 = e^2/4\pi\epsilon R$ and $E_C = E_{\text{tot}} - E_e - E_h - \hbar^2 K^2/2M$. To study the bound energy states of the exciton, we first have to determine the exciton potential. Examining equation (11), it is clear that evaluating this integral numerically is not straightforward because of the $1/r$ singularity for $r \to 0$.

The method we used to get rid of this problem is explained in the appendix. The result of the calculations can be found in figure 1, where we show the effective Coulomb potential when the electron and the hole are in the ground state, i.e. $\psi \to \psi_{0,0}$, ($V^{0,0}$) and in both the first and second excited state, i.e. $\psi \to \psi_{0,1}$ ($V^{0,1}$) and $\psi \to \psi_{0,2}$ ($V^{0,2}$) respectively (the single-particle densities are shown in figure 2). Notice how all effective potentials in figure 1 show the $-1/z$ behaviour for $z \to \infty$ and that the effective potential is finite for $z = 0$.

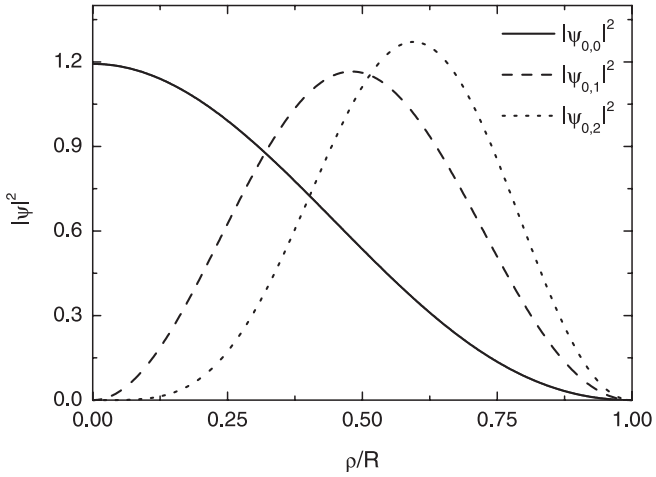

Figure 2. Density for the electron and hole in the nanowire for the lowest three single-particle states.

3.2. Approximate analytical expressions

Since the calculation of the effective Coulomb potential requires a considerable amount of computational time, it is highly desirable to have an analytical expression for it. Let us first consider the small-z behaviour of the effective potential:

$$\tilde{V}_{\mathrm{eff}}(z) = a + bz + cz^2, \tag{13}$$

where $\tilde{V}_{\mathrm{eff}}(z) = V_{\mathrm{eff}}(z)/E_0$ and z is in units of R. The coefficients are given by

$$a = \tilde{V}_{\mathrm{eff}}(z=0) = -2.5961, \tag{14}$$

$$b = \left.\frac{\mathrm{d}\tilde{V}_{\mathrm{eff}}(z)}{\mathrm{d}z}\right|_{z=0} = 4.1967, \tag{15}$$

$$c = \left.\frac{1}{2}\frac{\mathrm{d}^2\tilde{V}_{\mathrm{eff}}(z)}{\mathrm{d}z^2}\right|_{z=0} = -5.6140, \tag{16}$$

for the single-particle ground state. In a similar way, we get $a = -2.1126$ ($a = -1.9774$), $b = 3.1031$ ($b = 3.0608$) and $c = -4.5503$ ($c = -5.4277$) for the first (second) excited state. This polynomial expression, equation (13), is within 1% of the numerical result for $z/R < 0.14$.

Next we will look for an analytical expression that fits the whole range of z-values. Therefore, we have approximated the full effective potential by Padé approximants. The first Padé approximation is given by

$$\tilde{V}_{\mathrm{eff}}(z) = \frac{P_0(z)}{P_1(z)} = \frac{v}{w + |z|}, \tag{17}$$

where $P_i(z)$ is a polynomial of ith order. This formula corresponds to equation (2.8a) of [8]. If we take into account that $\tilde{V}_{\mathrm{eff}}(0) = v/w$ and remember that for $z \to \infty$ the effective potential behaves as a normal Coulomb potential $(-1/z)$, we can conclude that $v = -1$ and calculate that $w = 0.3852$ (ground state), $w = 0.4734$ (first excited state) and $w = 0.5057$ (second excited state).

This Padé approximation and the result of the calculations are compared in figure 3(a) for the ground state and in figure 3(b) for the first and second excited state.

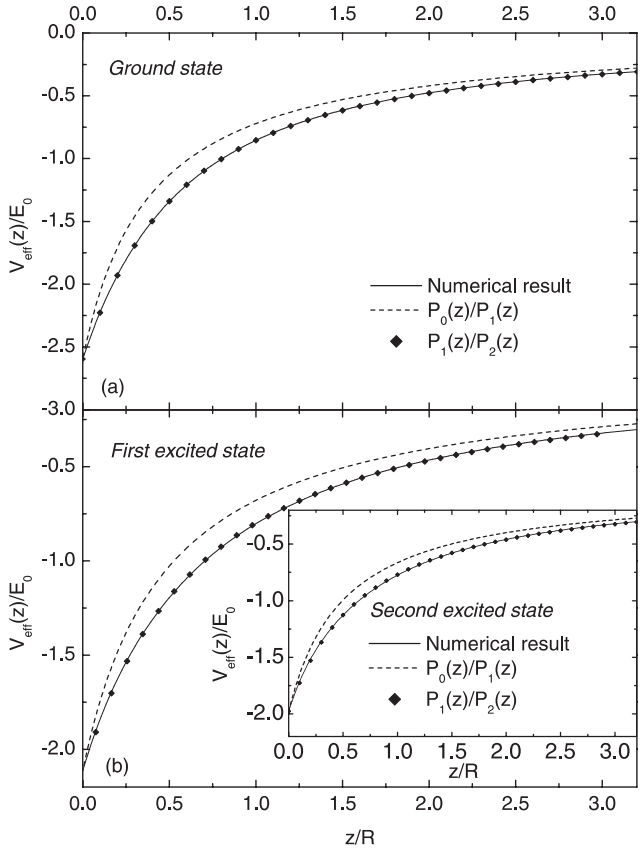

Figure 3. Plot of the numerical data and the two Padé approximations, $P_0(z)/P_1(z)$ and $P_1(z)/P_2(z)$, for (a) the ground state and (b) the first and second (inset) excited state.

To improve this result we consider the next Padé approximation:

$$\tilde{V}_{\text{eff}}(z) = \frac{P_1(z)}{P_2(z)} = \frac{\gamma\,|z| + \delta}{z^2 + \eta\,|z| + \beta}. \tag{18}$$

Again, there are certain conditions which impose restrictions on the values of the parameters. These conditions are $\tilde{V}_{\text{eff}}(z) \xrightarrow{z\to\infty} -1/z$, which implies that $\gamma = -1$ and $\delta/\beta = \tilde{V}_{\text{eff}}(z = 0)$, which leaves us with two fitting parameters. After fitting the data to the expression in equation (18), we find $\eta = 1.1288 \pm 0.0029$, $\beta = 0.4705 \pm 0.0015$, $\delta = -1.2215 \pm 0.0039$ for the electron and hole in the ground state, $\eta = 1.728 \pm 0.017$, $\beta = 0.899 \pm 0.011$, $\delta = 1.900 \pm 0.023$ for the electron and hole in the first excited state and $\eta = 2.749 \pm 0.061$, $\beta = 1.559 \pm 0.039$, $\delta = -1.9774\beta = 3.083 \pm 0.077$ for the electron and hole in the second excited state. The fitted second Padé approximation is also shown in figure 3, and we obtain an excellent fit (i.e. within 1.5%) for all states.

If the confinement potential for the electron and hole is a parabolic potential, i.e. $V(x, y) = m\omega_0^2(x^2+y^2)$, it is possible to perform all integrals in equation (11) analytically. The analytical result for the effective potential was obtained in [13] and reads

$$\tilde{V}_{\text{eff}}(z) = -\left(\frac{\pi}{2}\right)^{1/2} \frac{1}{l_0/R}\left[1 - \text{erf}\left(\frac{|z|}{\sqrt{2}l_0/R}\right)\right] \text{e}^{|z|^2/2(l_0/R)^2} \tag{19}$$

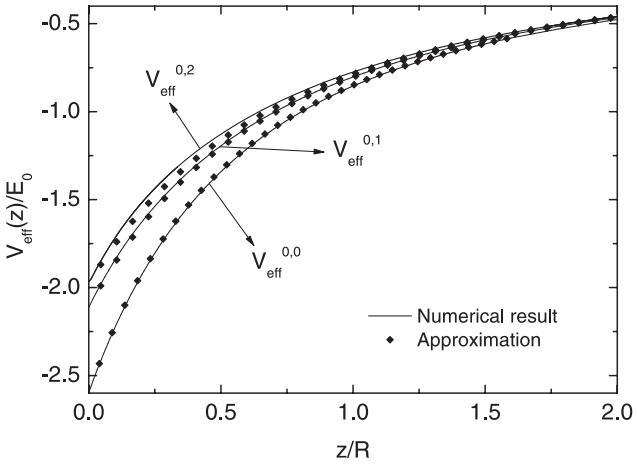

Figure 4. Comparison between the numerical effective electron–hole potential and the approximate one using the wavefunction of a harmonic oscillator for three different sets of quantum numbers of electron and hole.

with the oscillator length $l_0 = (\hbar/m\omega_0)^{1/2}$. It is remarkable that this potential approaches our effective exciton potential very closely if we define l_0 to be

$$l_0/R = -\frac{1}{\tilde{V}_{\text{eff}}(0)}\left(\frac{\pi}{2}\right)^{1/2} \tag{20}$$

i.e. the expression for the oscillator length extracted from equation (19) by putting $z = 0$. It is possible now to calculate l_0/R numerically for the different effective potentials: $l_0/R = 0.4828$ (ground state), $l_0/R = 0.5933$ (first excited state) and $l_0/R = 0.6338$ (second excited state). Using these results in equation (19), we get an expression for the effective exciton potential as a function of the interparticle distance. The approximation and the calculated data can be seen in figure 4, and they show a good agreement for the ground state and first excited state (fit within 0.7% of the data), while for the second excited state the approximated result is still reasonable (fits within 3.2% of the data).

4. Exciton energy

4.1. Numerical calculations

When a single exciton is created by excitation, its energy is generally given by $E = E_g + E_e + E_h + E_C$, where E_g denotes the energy band gap, $E_{e(h)}$ is the single-electron (hole) energy and E_C is the (negative) energy of the Coulomb interaction between the electron and hole. For a given material, we have to calculate now E_C; all other contributions to the exciton energy are known. Therefore, the 1D Schrödinger equation (equation (12)) was solved using the finite difference technique. Figure 5 shows the energy of the Coulomb interaction of the three lowest exciton energy levels as a function of the dimensionless parameter $\alpha = a_B^*/2R$ for two cases of the effective potential.

The binding energy can also be fitted to an analytical expression now. Values of $\alpha < 0.1$ are not realistic, since this would correspond to a large radius and a strong confinement approach would no longer be valid. Therefore, the following fit is suggested for α-values

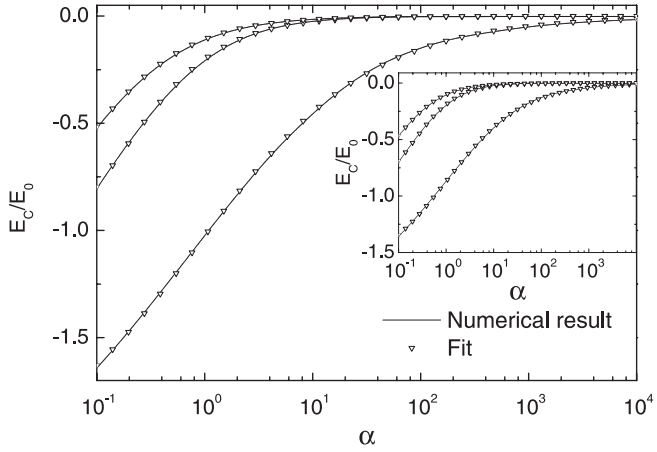

Figure 5. Binding energy as a function of the parameter $\alpha = a_B^*/2R$. The solid curves are calculated by using the effective potential $V^{0,0}$ (electron and hole in the ground state). The symbols represent the fit which is given by equation (21). Inset: the same, but now for the effective potential $V^{0,1}$ (electron and hole in the first excited state).

exceeding 0.1:

$$\tilde{E}_C = \frac{\xi}{1 + b\alpha^\tau}. \tag{21}$$

For the ground state configuration of the electron and hole, we find that $\xi = -2.145 \pm 0.020$, $b = 1.093 \pm 0.022$, $\tau = 0.5385 \pm 0.0040$, and for the first (second) excited states of the exciton binding energy we find $\xi = -1.287 \pm 0.031$, $b = 5.42 \pm 0.16$ and $\tau = 0.945 \pm 0.013$ ($\xi = -1.211 \pm 0.016$, $b = 10.23 \pm 0.14$ and $\tau = 0.8830 \pm 0.0034$) (see figure 5 for the fits). Similarly, for the configuration where the electron and hole are in the first excited state, we find that $\xi = -1.714 \pm 0.015$, $b = 0.967 \pm 0.020$ and $\tau = 0.5449 \pm 0.0042$ (ground state), $\xi = -1.0525 \pm 0.028$, $b = 4.56 \pm 0.16$, $\tau = 0.940 \pm 0.016$ (first excited state) and $\xi = -0.965 \pm 0.016$, $b = 8.47 \pm 0.15$, $\tau = 0.8944 \pm 0.0051$ (second excited state).

From equation (12) it is clear that, for small α-values, there is a relatively smaller contribution of the kinetic energy term $\nabla_z^2\psi$. As α increases, the energy of the particle will also increase, because of an increase in the contribution from the kinetic energy term. For large values of α the energy levels become closely packed to the $\tilde{E}_C = 0$ level. In fact, because of the $1/z$ behaviour of the exciton potential for large z, the integral $\int V(z)^{1/2}\,dz = \infty$ and according to [16] there will be an infinite number of bound states.

4.2. Comparison with analytical results

In this section we present an analytical solution of the 1D Schrödinger equation (12). Similar calculations were done earlier by Loudon [17], who solved the problem of the 1D hydrogen atom (i.e. the ideal limit of the 1D electron–hole system: infinitesimal wire cross-section and hard wall confinement) analytically. To avoid the divergence of the original potential at $z = 0$ Loudon used different models, e.g. hard wall conditions at $z = 0$, i.e. $\phi(z = 0) = 0$. The 1D Schrödinger equation, equation (12), has in general to be solved numerically. We used the finite difference technique. In the special case in which the effective potential is approximated by the first Padé approximant, equation (17), it is possible to obtain an analytical expression for the wavefunction. After introducing the new variable $y = 2\sqrt{-\tilde{E}_C/\alpha}(z + w)$, we can rewrite

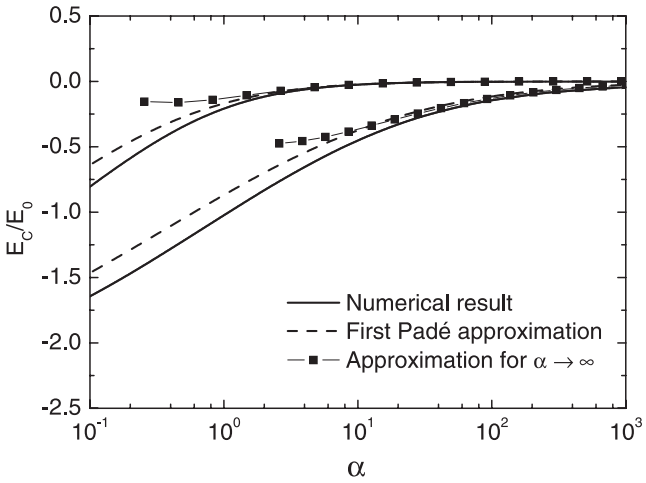

Figure 6. Ground state (lower curves) and first excited state (upper curves) energy of the exciton when using (1) the first Padé approximation for the electron–hole interaction potential and (2) the numerical expression for the electron and hole in the ground state. The curve with symbols is the asymptotic behaviour, i.e. equation (25).

equation (12) as the Whittaker equation:

$$\nabla_y^2\phi(y) + \left(-\frac{1}{4} + \frac{-v}{2y\alpha\sqrt{-\tilde{E}_C/\alpha}}\right) = 0. \tag{22}$$

The wavefunctions are then given in terms of the Whittaker function

$$\phi(y) = Ay\mathrm{e}^{-y/2}U(1-\kappa;2;y), \tag{23}$$

where A is a normalization constant and $\kappa = -v/2\alpha\sqrt{-\tilde{E}_C/\alpha}$. The energy is then obtained by solving the following equations:

$$\left.\frac{\mathrm{d}\phi(y)}{\mathrm{d}y}\right|_{y=2w\sqrt{-\tilde{E}_C/\alpha}} = 0 \qquad \text{(even states)},$$
$$\phi\left(y = 2w\sqrt{-\tilde{E}_C/\alpha}\right) = 0 \qquad \text{(odd states)}. \tag{24}$$

We now obtain the energy of the Coulomb interaction semi-analytically (by solving the transcendent equation) and we compare it in figure 6 with the numerically calculated energy. Notice that for large α both energies are close to each other. But for small α-values (which corresponds to large R) there is a underestimation of the exciton energy up to 15%. This is not surprising, since the first Padé approximation leads to a rather poor fit to the effective potential (see figure 3(a)). Nevertheless analytical calculations are useful because they allow for an estimation of the energy without having to solve the differential equation (12) numerically. Furthermore it has to be noticed that, in the case of large α (which corresponds to small radii R), it is now possible to find a simple analytical expression [8] for $\tilde{E}_C$, i.e.

$$\tilde{E}_C = -1/4\,\alpha v^2 \tag{25}$$

where

$$v = v_m \begin{cases} v_m = m + \dfrac{w}{\alpha} & \text{(odd states)} \\ v_m = m - \dfrac{1}{\ln(w/m\alpha)} & \text{(even states)} \end{cases} \tag{26}$$

for $m = 1, 2, 3, \ldots$. These correspond to the bound states of the exciton. This asymptotic result is shown in figure 6 by the square symbols and is clearly only valid for large α. Note that in the limit of a Coulomb interaction potential the excited states are twofold degenerate. The lowest bound state satisfies the special relation

$$\ln\left(\frac{w}{\nu_0\alpha}\right) + \frac{1}{2\nu_0} = 0. \tag{27}$$

This approximation is also shown in figure 6.

5. Magnetic field dependence

5.1. Single-particle properties

When a magnetic field, directed along the wire, is applied, the single-particle Hamiltonian for an electron ($q = -|e|$) or hole ($q = |e|$) can be written as

$$H = \frac{1}{2m}\left(-\mathrm{i}\hbar\vec{\nabla} - q\vec{A}\right)^2 + V(\vec{r}), \tag{28}$$

where $V(\vec{r})$ is again the confinement potential of the wire. Due to the symmetry of the problem we may benefit from the symmetric gauge $\vec{A} = \frac{1}{2}B\rho\vec{e}_\theta$ for the vector potential. For the same reason, the wavefunction $\psi(\rho, \theta)$ is separable, and it can be written as $\psi(\rho, \theta) = R(\rho)\mathrm{e}^{-\mathrm{i}l\theta}$, where the z-dependence has been omitted for the sake of simplicity. The Schrödinger equation now reads

$$\left(\frac{\partial^2}{\partial\rho^2} + \frac{1}{\rho}\frac{\partial}{\partial\rho} - \frac{l^2}{\rho^2}\right)R + \left(-\frac{m\omega_c}{\hbar}\mathrm{sgn}\,(q)l - \left(\frac{m\omega_c}{2\hbar}\right)^2\rho^2 + \frac{2mE}{\hbar^2}\right)R = 0, \tag{29}$$

where $\omega_c = |e|\,B/m$ is the cyclotron frequency. Introducing the following parameters, $k^{*^2} = -\mathrm{sgn}\,(q)lm\omega_c/\hbar + 2mE/\hbar^2$ and $1/l_B^2 = m\omega_c/2\hbar$, and by putting $R(\rho) = \rho^{|l|}\exp(-\rho^2/2l_B^2)f(\rho)$, one gets

$$tf'' + ((|l|+1) - t)f' - \left(\frac{1}{2}(|l|+1) - \frac{l_B^2k^{*^2}}{4}\right)f = 0, \tag{30}$$

where the new variable t is given by $t = \rho^2/l_B^2$. The solution is the confluent hypergeometric function [18].

$$\psi_{n,l}(\rho, \theta) = C_{n,l}\mathrm{e}^{-\mathrm{i}l\theta}\rho^{|l|}\mathrm{e}^{-\frac{\rho^2}{2l_B^2}}{}_1F_1\left(-a_{n,l};\,|l|+1;\,\frac{\rho^2}{l_B^2}\right), \tag{31}$$

where $C_{n,l}$ is a normalization constant and

$$-a_{n,l} = \frac{1}{2}(|l|+1) - \frac{l_B^2k^{*^2}}{4}, \tag{32}$$

is a constant which is obtained by using the hard wall boundary conditions, i.e. $\psi_{n,l}(R, \theta) = 0$. The single-particle energy then becomes

$$E_{n,l} = \hbar\omega_c\left(a_{nl} + \frac{1 + |l| + \mathrm{sgn}(q)l}{2}\right). \tag{33}$$

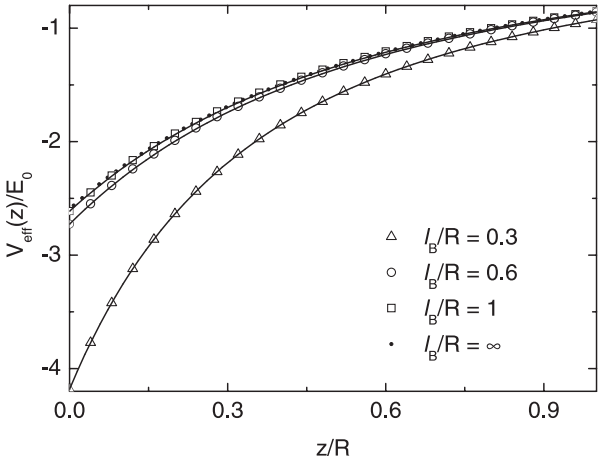

Figure 7. Effective exciton potential for different values of the magnetic field (full lines) in which the electron and hole are in the ground state. The approximation (open symbols) of equation (19) can be used again to fit the calculated effective potential. For comparison, the effective potential for the system without magnetic field was also drawn ($l_B/R = \infty$, dotted line). Note that, for this figure, the electron and hole were in the ground state.

5.2. Effective exciton potential

The total Hamiltonian is now given by

$$H_{\text{tot}} = -\frac{1}{2m_{\text{e}}}\left(\vec{p}_{x_{\text{e}},y_{\text{e}}} + |e|\,\vec{A}\right)^2 + V_{\text{e}}(x_{\text{e}}, y_{\text{e}}) - \frac{1}{2m_{\text{h}}}\left(\vec{p}_{x_{\text{h}},y_{\text{h}}} - |e|\,\vec{A}\right)^2 + V_{\text{h}}(x_{\text{h}}, y_{\text{h}}) - \frac{\hbar^2}{2m_{\text{e}}}\nabla^2_{z_{\text{e}}} - \frac{\hbar^2}{2m_{\text{h}}}\nabla^2_{z_{\text{h}}} - \frac{1}{4\pi\epsilon}\frac{e^2}{\sqrt{(x_{\text{e}}-x_{\text{h}})^2 + (y_{\text{e}}-y_{\text{h}})^2 + z^2}}. \tag{34}$$

Again, we can reduce this equation to a 1D effective Schrödinger equation similarly as for the $B = 0$ case (i) by separating the motion of the two particles into the centre of mass relative coordinates, (ii) by using the adiabatic approximation for the exciton wavefunction, and (iii) by introducing the same dimensionless units as in section 3.1. This leads us to the equivalent of equation (12), where the single-particle energies are now given by equation (33) and the averaging of the effective potential has to be performed with the Kummer functions (equation (31)) (instead of Bessel functions). Note that the confluent hypergeometric function ${}_1F_1$ is equivalent to the Kummer function M:

$${}_1F_1(a; b; z) = M(a, b, z). \tag{35}$$

Figure 7 shows the effective potential for different values of the magnetic field (which corresponds to different values of the magnetic length $l_B = \sqrt{2\hbar/m\omega_c}$). These potentials can be approximated again by the expression in equation (19) (see the fit in figure 7). Therefore it is more interesting to determine the relation between l_B and $\tilde{V}_{\text{eff}}(z = 0)$, since the value of $\tilde{V}(z = 0)$ will enable us to calculate l_0/R (equation (20)) and therefore to reconstruct the effective potential for the whole range of z-values for an arbitrary magnetic field. Figure 8 shows this curve for both the electron and hole in the ground state and in the first excited state.

This figure can be understood as follows. Large values of l_B correspond to the absence of a magnetic field and therefore the curve converges to the previously calculated value of $\tilde{V}_{\text{eff},l_B\to\infty}(z = 0)$ for $B = 0$. For small values of l_B, equation (19) matches the calculated curve,

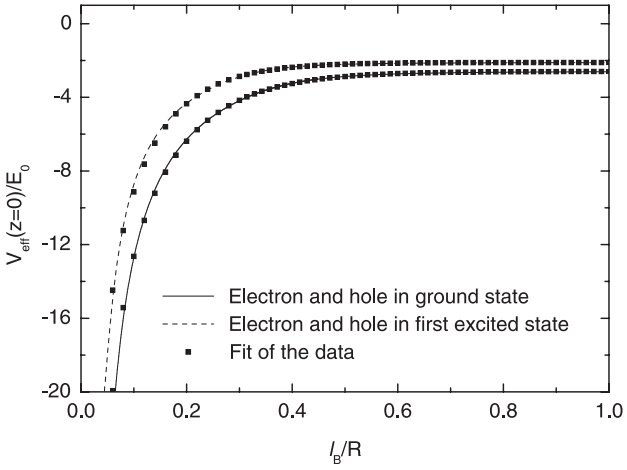

Figure 8. Effective exciton potential at $z = 0$ as function of the magnetic length l_B (the magnetic field). The fit is to equations (37) and (39).

because for high magnetic fields, the confinement becomes effectively parabolic. Replacing the oscillator length l_0 by l_B, the result for large magnetic fields is recovered:

$$\tilde{V}^{0,0}_{\mathrm{eff},l_B\to 0}(z=0) = -\sqrt{\frac{\pi}{2}}\frac{1}{l_B/R}. \tag{36}$$

Putting together these results into a single formula, we obtain a fit for the effective potential as a function of the magnetic field:

$$\tilde{V}^{0,0}_{\mathrm{eff}}(z=0) = \tilde{V}^{0,0}_{\mathrm{eff},l_B\to\infty}(z=0) - \sqrt{\frac{\pi}{2}}\frac{1}{\tilde{l}/R}\mathrm{e}^{-pl_B}, \tag{37}$$

where $1/\tilde{l}^2 = 1/l_0^2 + 1/l_B^2$. Two parameters have been determined by fitting the data, and they are $l_0/R = 0.0624 \pm 0.0021$ and $pR = 8.570 \pm 0.090$ for the electron and the hole in the ground state configuration. Notice that basically we used the expression for the parabolic confinement equation (19), and by rescaling l_0 to $\tilde{l}$, we include the effect of the magnetic field.

By making a similar calculation to the one in [13], but for the electron and hole in the first excited state, we find that

$$\tilde{V}^{0,1}_{\mathrm{eff},l_B\to 0}(z=0) = -\frac{11}{16}\sqrt{\frac{\pi}{2}}\frac{1}{l_B/R}. \tag{38}$$

Therefore we fitted the data for $|n_\mathrm{e}, l_\mathrm{e}\rangle = |n_\mathrm{h}, l_\mathrm{h}\rangle = |n, l\rangle = |0, 1\rangle$ to a slightly different function,

$$\tilde{V}^{0,1}_{\mathrm{eff}}(z=0) = \tilde{V}^{0,1}_{\mathrm{eff},l_B\to\infty}(z=0) - \frac{11}{16}\sqrt{\frac{\pi}{2}}\frac{1}{\tilde{l}/R}\mathrm{e}^{-pl_B}, \tag{39}$$

where $l_0/R = 0.0462 \pm 0.0026$ and $pR = 10.73 \pm 0.17$. The numerical results together with the results of the fit are shown in figure 8, and they agree very well.

5.3. Exciton energy

Previously, we calculated the exciton energy as a function of the dimensionless parameter $\alpha = a^*_\mathrm{B}/2R$, which is determined by the wire radius and the material parameters. In this

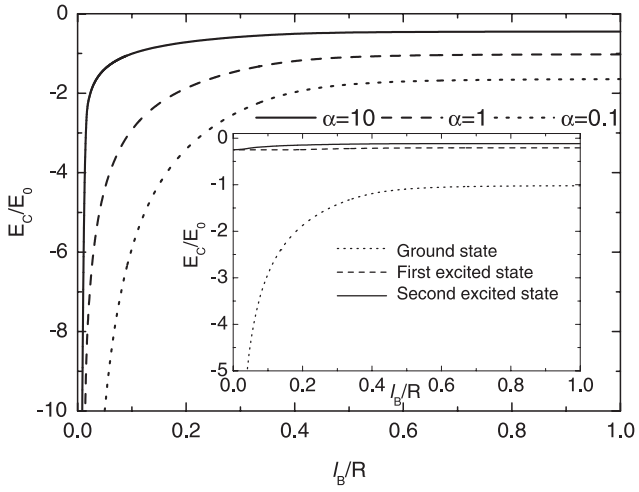

Figure 9. Ground state exciton binding energy for the electron and hole in the ground state as a function of the magnetic length $l_B = \sqrt{2\hbar/eB}$ for different values of α. Inset: the same but now for the ground state, first and second excited state with $\alpha = 1$.

case, there is another variable which can be changed and will have an effect on the energy: the magnetic length l_B. Considering the previous results of the system without magnetic field and knowing that the shape of the potential does not fundamentally change by applying a magnetic field (the effective potential well only gets deeper), we also know that the energy as a function of α will not give a fundamentally different result from the previous one. Therefore we calculated the binding energy as a function of the magnetic field (or the magnetic length l_B) for a few fixed values of α ($\alpha = 10$, $\alpha = 1$ and $\alpha = 0.1$) and the result of these calculations can be seen in figure 9. The main figure shows only the ground state binding energy, while the inset shows also the energy of the first and second excited state. The inset shows that the magnetic field influences the ground state more than the first and second excited states, which are almost constant. For high magnetic fields, which corresponds to $l_B/R \to 0$, we find that the effective potential of equation (19) becomes a $1/z$-potential [15]. This means that we can use equations (25)–(27) again to determine the asymptotic behaviour of $\tilde{E}_C$ as function of l_B. We find that the ground state energy $\tilde{E}_C \to \infty$ for $l_B \to 0$ for all values of α, whereas for $\alpha = 1$ (inset of figure 9) the first and second excited state become, in the limit $B \to \infty$, degenerate with energy $-1/4$.

6. Conclusion

In summary, we have calculated the effective interaction potential and the binding energy for an exciton in a nanowire. The effective interaction potential was calculated for different states of the electron and hole and we were able to present 'exact' numerical results. In order to reduce the amount of computational time for future calculations, these results were used to propose various analytical approximate expressions. We fitted the results to three different functions. A first Padé approximation gives the correct qualitative behaviour, but the fit was not optimal. Nevertheless this expression was useful to perform further analytical calculations to estimate the binding energy of the exciton, especially for small values of the wire radius R. A second Padé approximation as well as the result from the parabolic confinement resulted in very

good fits. Furthermore the exciton binding energy was calculated both semi-analytically and numerically, and analytical approximations were given. We also investigated the influence of a magnetic field and determined an analytical expression for the effective potential for arbitrary magnetic field values. Finally we calculated the binding energy as a function of the magnetic field, where we found that the ground state binding energy is most affected by a variation of the magnetic field.

Acknowledgments

This work was supported by the Flemish Science Foundation (FWO-Vl), the Belgian Science Policy, the EU network of excellence: SANDiE and the UA-IMEC, vzw collaborative project.

Appendix. Numerical calculation of the effective potential

To obtain the effective exciton potential of equation (11), we have to evaluate four-fold integrals. They can be rewritten in polar coordinates as follows, using the same dimensionless units as before:

$$V_{\mathrm{eff}}(z) = -R^4 \int \rho_\mathrm{e}\rho_\mathrm{h}\,\mathrm{d}\rho_\mathrm{e}\,\mathrm{d}\rho_\mathrm{h}\,\mathrm{d}\theta_\mathrm{e}\,\mathrm{d}\theta_\mathrm{h} \frac{|\psi_{nl}(R\rho_\mathrm{e},\theta_\mathrm{e})|^2\,|\psi_{n'l'}(R\rho_\mathrm{h},\theta_\mathrm{h})|^2}{\sqrt{\rho_\mathrm{e}^2+\rho_\mathrm{h}^2-2\rho_\mathrm{e}\rho_\mathrm{h}\cos(\theta_\mathrm{e}-\theta_\mathrm{h})+z^2}}. \tag{A.1}$$

Due to cylindrical symmetry, we can perform the integral over the angle θ_h analytically, yielding

$$\begin{aligned}\int_0^{2\pi}\mathrm{d}\theta_\mathrm{e}\int_0^{2\pi}&\frac{\mathrm{d}\theta_\mathrm{h}}{\sqrt{\rho_\mathrm{e}^2+\rho_\mathrm{h}^2-2\rho_\mathrm{e}\rho_\mathrm{h}\cos(\theta_\mathrm{e}-\theta_\mathrm{h})+z^2}}\\ &= 2\pi\frac{4}{\sqrt{(\rho_\mathrm{e}+\rho_\mathrm{h})^2+z^2}}\mathbb{K}\left(\frac{4\rho_\mathrm{e}\rho_\mathrm{h}}{(\rho_\mathrm{e}+\rho_\mathrm{h})^2+z^2}\right)\end{aligned} \tag{A.2}$$

where $\mathbb{K}(m)$ is the elliptic integral of the first kind. Using a polynomial approximation [15] for the elliptic integral,

$$\begin{aligned}\mathbb{K}(m) &= \sum_{i=0}^{4} a_i m_1^i + \sum_{i=0}^{4} b_i m_1^i \ln\frac{1}{m_1}\\ &\equiv \mathbb{A}(m_1)+\mathbb{B}(m_1)\ln(1/m_1),\end{aligned} \tag{A.3}$$

with $m_1 = 1-m$, we find that

$$\begin{aligned}V_{\mathrm{eff}}(z) = -2\pi R^4 &\int_0^1 \mathrm{d}\rho_\mathrm{e}\rho_\mathrm{e}\,|\psi_{nl}(R\rho_\mathrm{e},\theta_\mathrm{e})|^2\\ &\times \underbrace{\int_0^1 4\frac{\mathrm{d}\rho_\mathrm{h}\rho_\mathrm{h}\,|\psi_{n'l'}(R\rho_\mathrm{h},\theta_\mathrm{h})|^2}{\sqrt{(\rho_\mathrm{e}+\rho_\mathrm{h})^2+z^2}}\left[\mathbb{A}(m_1)+\mathbb{B}(m_1)\ln\frac{1}{m_1}\right]}_{\equiv I_1}.\end{aligned}$$

In a next step, we calculate the integral I_1 over r_h using numerical techniques. To obtain good convergence, we use the logarithmically weighted method and consider the following integral:

$$I(\rho_\mathrm{e},z) = \int_0^1 \mathrm{d}\rho_\mathrm{h} F(\rho_\mathrm{h},\rho_\mathrm{e},z)\ln\left(\frac{(\rho_\mathrm{e}-\rho_\mathrm{h})^2+z^2}{(\rho_\mathrm{e}+\rho_\mathrm{h})^2+z^2}\right). \tag{A.4}$$

We use the following transformation:

$$I(\rho_e, z) = \sum_{i=0}^{s-1} \int_0^h dx\, F(x + hi, \rho_e, z) \ln\left(\frac{(x - (\rho_e - hi))^2 + z^2}{(x + (\rho_e + hi))^2 + z^2}\right), \tag{A.5}$$

where h denotes the step size and s the total number of steps. If we replace $F(x + hi)$ by $F_i + (F_{i+1} + F_i)x/h$, we can write (A.5) as

$$I(\rho_e, z) = \sum_{i=0}^{s-1} F_i A_i(\rho_e, z) + (F_{i+1} - F_i)\, C_i(\rho_e, z), \tag{A.6}$$

and the remaining problem is the calculation of the coefficients A_i and C_i. These coefficients are given by

$$\begin{aligned} A_i(\rho_e, z) &= \int_0^h dx \ln\left(\frac{(x - (\rho_e - hi))^2 + z^2}{(x + (\rho_e + hi))^2 + z^2}\right), \\ C_i(\rho_e, z) &= \frac{1}{h}\int_0^h dx\, x \ln\left(\frac{(x - (\rho_e - hi))^2 + z^2}{(x + (\rho_e + hi))^2 + z^2}\right). \end{aligned} \tag{A.7}$$

These integrals can be performed analytically, which leads to the following results:

$$A_i(\rho_e, z) = a(h - (\rho_e - hi)) - a(h + (\rho_e + h_i)), \tag{A.8}$$

$$C_i(\rho_e, z) = h^{-1}\left[c(h - (\rho_e - hi)) - c(h + (\rho_e + h_i))\right] - 2r_e, \tag{A.9}$$

with

$$\begin{aligned} a(y) &= H_i(y) + H_i(h - y) + 2z\left[\arctan\left(\frac{y}{z}\right) + \arctan\left(\frac{h - y}{z}\right)\right], \\ H_i(y) &= y \ln(y^2 + z^2), \\ c(y) &= \tfrac{1}{2}\left(y(2h - y) + z^2\right) G_i(y) + \tfrac{1}{2}\left((h - y)^2 - z^2\right) G_i(h - y) 2z(h - y) \\ &\quad \times \left[\arctan\left(\frac{y}{z}\right) + \arctan\left(\frac{h - y}{z}\right)\right], \\ G_i(y) &= \ln(y^2 + z^2). \end{aligned} \tag{A.10}$$

Now we can write, using the logarithmically weighted method,

$$\begin{aligned} I_1 &= \int \frac{4 d\rho_h \rho_h \left|\psi_{n'l'}(R\rho_h, \theta_h)\right|^2}{\sqrt{(\rho_e + \rho_h)^2 + z^2}} \left(\mathbb{A}(m_1) + \mathbb{B}(m_1)\ln(m_1)\right) \\ &= \sum_{i=0}^{s-1} \int_0^h dx\, F(x + hi)\left(\mathbb{A}(m_1) + \mathbb{B}(m_1)\ln(m_1)\right) \\ &= \sum_{i=1}^{s-1} \left(F_i h \mathbb{A}(m_1) + F_i\left(A_i + C_{i-1} - C_i\right)\mathbb{B}(m_1)\right) \\ &\quad + F_s \frac{h}{2}\mathbb{A}(m_1) + F_s C_{s-1}\mathbb{B}(m_1), \end{aligned} \tag{A.11}$$

where

$$F_i \equiv F(hi) = \frac{4hi\left|\psi_{n',l'}(Rhi, \theta_h)\right|^2}{\sqrt{(\rho_e + hi)^2 + z^2}}. \tag{A.12}$$

The final step is then to calculate the integral over ρ_e. Similarly, we can also perform this last integration over ρ_e. Using the above-mentioned result of equation (A.11), we obtain the final expression for the effective potential in the z-direction:

$$V_{\text{eff}}(z) = -\frac{2\pi}{N^2}R^4\Bigg[h\sum_{j=1}^{s-1} hj\,|\psi_{nl}(Rhj,\theta_e)|^2\Bigg[\Bigg[S_1(hj)h + T(hj)\frac{h}{2}\mathbb{A}(m_1)\Bigg] - \big[S_2(hj) + T(hj)C_{s-1}\mathbb{B}(m_1)\big]\Bigg] + \frac{h}{2}hs\,|\psi_{nl}(Rsh,\theta_e)|^2 \times \Bigg[\Bigg[S_1(hs)h + T(hs)\frac{h}{2}\mathbb{A}(m_1)\Bigg] - \big[S_2(hs) + T(hs)C_{s-1}\mathbb{B}(m_1)\big]\Bigg]\Bigg]$$

with

$$S_1(x) = \sum_{i=1}^{s-1}\frac{4hi\,|\psi_{n'l'}(Rhi,\theta_h)|^2}{\sqrt{(x+hi)^2+z^2}}\mathbb{A}(m_1), \tag{A.13}$$

$$T(x) = \frac{4sh\,|\psi_{n'l'}(Rsh,\theta_h)|^2}{\sqrt{(x+sh)^2+z^2}}, \tag{A.14}$$

$$S_2(x) = \sum_{i=1}^{s-1}\frac{4hi\,|\psi_{n'l'}(Rhi,\theta_h)|^2}{\sqrt{(x+hi)^2+z^2}}(A_i + C_{i-1} - C_i)\mathbb{B}(m_1). \tag{A.15}$$

References

[1] Morales A M and Lieber C M 1998 *Science* **279** 208
[2] Duan X, Huang Y, Cui Y and Lieber C M 2002 *Nano Lett.* **2** 101
[3] Cui Y and Lieber C M 2001 *Science* **291** 851
[4] Duan X, Huang Y and Lieber C M 2002 *Nano Lett.* **2** 487
[5] Huang M H, Mao S, Feick H, Yan H, Wu Y, Weber E, Russo R and Yang P 2001 *Science* **292** 1897
[6] Duan X, Huang Y, Agarwal R and Lieber C M 2003 *Nature* **421** 241
[7] Cui Y, Wei Q, Park H and Lieber C M 2001 *Science* **293** 1289
[8] Ogawa T and Takagahara T 1991 *Phys. Rev.* B **44** 8138
[9] Chuu D S, Hsiao C M and Mei W N 1992 *Phys. Rev.* B **46** 3898
[10] Branis S V, Li G and Bajaj K K 1993 *Phys. Rev.* B **47** 1316
[11] Banyai L, Galbraith I, Ell C and Haug H 1987 *Phys. Rev.* B **36** 6099
[12] Sidor Y, Partoens B and Peeters F M 2005 *Phys. Rev.* B **71** 165323
[13] Bednarek S, Szafran B, Chwiej T and Adamowski J 2003 *Phys. Rev.* B **68** 045328
[14] Zhang Y and Mascarenhas A 1999 *Phys. Rev.* B **59** 2040
[15] Abramowitz M and Stegun I 1970 *Handbook of Mathematical Functions* (New York: Dover) p 295, 409, 590
[16] Price P J 1996 *Solid State Electron.* **39** 653
[17] Loudon R 1959 *Am. J. Phys.* **27** 649
[18] Geerinckx F, Peeters F M and Devreese J T 1990 *J. Appl. Phys.* **68** 3435